Available online at www.sciencedirect.com

ScienceDirect

Energy Procedia 155 (2018) 503–513

Energy Procedia

www.elsevier.com/locate/procedia

12th International Renewable Energy Storage Conference, IRES 2018

Molten salt chemistry in nitrate salt storage systems: Linking experiments and modeling

Veronika Anna Sötz[a]*, Alexander Bonk[b], Jochen Forstner[b], Thomas Bauer[a]

[a]*Institute of Engineering Thermodynamics, German Aerospace Center (DLR), Linder Höhe, 51147 Köln, Germany*
[b]*Institute of Engineering Thermodynamics, German Aerospace Center (DLR), Pfaffenwaldring 38-40, 70569 Stuttgart, Germany*

Abstract

Sensible heat storage in molten nitrate salts is a key technology when it comes to thermal energy storage in combination with concentrating solar power (CSP) plants. Currently, a mixture of sodium and potassium nitrate called Solar Salt is used at temperatures between 280 and 560 °C. Our research approaches comprise an improvement of Solar Salt stability at temperatures above 560 °C, which comes along with a broadening of the operating temperature range. In this way, a higher storage capacity and efficiency, as well as economic advances can be achieved. Numerous publications about the chemistry of molten nitrate salt mixtures reveal the formation of chemical species such as nitrite ions, nitrous gases and oxide ions and carbonate ions. Among these, the reversible reaction of nitrate to nitrite with release of oxygen is the predominant reaction at temperatures below 560 °C. So far, there is a lack of literature that pays particular attention on the contributions of reaction kinetics and mass transport effects on the reaction velocity of the nitrate/nitrite-reaction. However, understanding of these physico-chemical phenomena is essential, because further decomposition reactions build on the nitrate/nitrite-reaction. In this study, experiments at different scales (50 mg to 100 g) are compared with regard to the reduction reaction velocity at 500 °C. A data treatment procedure for thermogravimetric analysis experiments successfully eliminates effects of salt evaporation on the measured mass changes. The chemical equilibrium of the salt samples turned out to be reasonable, when compared to literature values. It was found, that the surface-to-volume ratio of the salt melt samples significantly affects the evaporation rates and the reaction velocity. The time period that is needed until chemical equilibrium is reached at 500 °C clearly increases when the surface-to-volume ratio decreases. The thermogravimetric analysis apparatus enables experiments, which measure reaction kinetics without mass transport limitations. It is demonstrated that a simulation model adapted from literature displays a reaction velocity that incorporates both reaction kinetics and mass transport without differentiation of the two phenomena.

* Corresponding author. Tel.: +49-2203-601-3606.
E-mail address: Veronika.Soetz@dlr.de

1876-6102
10.1016/j.egypro.2018.11.030

Keywords: Sensible heat storage; nitrate salt melt; thermal decomposition; nitrous gases; kinetics; modeling

1. Introduction

The present study concerns the chemistry in molten nitrate salt. It is relevant for the field of energy storage, more precisely for sensible heat storage with nitrate salt melts as heat storage material and heat transfer fluid (HTF). The investigated material Solar Salt is a mixture of sodium nitrate ($NaNO_3$, 60 wt.%) and potassium nitrate (KNO_3, 40 wt.%). It is already applied as HTF and heat storage material in concentrating solar power (CSP) plants [1]. At the moment, the operation temperature ranges from about 290 to 560 °C. One of the current research intentions is to raise the maximum operating temperature [2], which can lead to a higher storage capacity, a higher efficiency of the heat to power conversion, and faster salt heating, e.g. in smaller sized heat exchangers in the receiver unit of a CSP plant. Eventually, the temperature raise is expected to result in a better economic performance of the molten salt storage and CSP systems. To enable higher operating temperatures, it is mandatory to enhance the stability of Solar Salt at high temperatures. Solar salt heating comes along with different decomposition reaction, e.g. nitrite formation in the melt with oxygen release, and oxide formation with release of nitrous oxides. This paper focuses on the velocity of the nitrite ion formation including the relevant physical chemical factors.

A large number of reaction equations was published in the past with the intention to explain the formation of species, which are observable in molten nitrate salts and in the overlying gas atmosphere. These include nitrite (NO_2^-) and oxide (O^{2-}) ions, as well as gases such as oxygen (O_2) and nitrous gases (e.g. NO and N_2O, see equations (2), (3), (4) [3–6]). However, only reaction (1) is generally accepted, and it describes the conversion of nitrate ions to nitrite ions and oxygen, and vice versa.

$$NO_3^- \rightleftharpoons NO_2^- + 0.5\ O_2 \tag{1}$$

$$2\ NO_2^- \rightleftharpoons NO_3^- + 2\ O^{2-} + 2\ NO + N_2 \tag{2}$$

$$2\ NO_2^- \rightleftharpoons O^{2-} + 2\ NO + 0.5\ O_2 \tag{3}$$

$$2\ NO_2^- \rightleftharpoons O^{2-} + N_2O + O_2 \tag{4}$$

The thermodynamics of reaction (1) were studied experimentally with regard to the chemical equilibrium (see Table 1). The equilibrium constant $K_{(1),T}$ at a certain temperature can be calculated with the equilibrium concentrations $c_{i,eq,T}$ of the species i that participate in the reaction and the oxygen partial pressure $p_{O_2,eq}$, according to equation (5). In the case of the nitrate/nitrite-reaction, the quotient of the equilibrium concentrations of nitrate and nitrite $\frac{c_{NO_3^-,eq,T}}{c_{NO_2^-,eq,T}}$ is equal to the ratio of the amounts of substance $\frac{n_{NO_3^-,eq,T}}{n_{NO_2^-,eq,T}}$, which is abbreviated with $x_{(1),T,p_{O_2}}$ in this study. The equilibrium constants are linked to the enthalpy ΔH and entropy ΔS of the regarded reaction (equation (6)). The enthalpy ΔH and entropy ΔS are extracted from the experimentally measured equilibrium constants at different temperatures via equation (6). The equilibrium constants at 500 °C $K_{(1),500}$ vary from 35 to 276 $atm^{-0.5}$. The values obtained from the two publications that consider similar cation compositions [19,20] amount to 178 and 101 $atm^{-0.5}$(Table 1, column 5), respectively. The corresponding molar ratios nitrate-to-nitrite in a melt at 500 °C and in thermodynamic equilibrium with synthetic air $x_{(1),500,0.2}$ (see Table 1, column 6) differ by a factor of almost 2 (80

and 45 mol·mol^{-1}, respectively).

$$K_{(1),T} = \frac{c_{NO_3^-,eq,T}}{c_{NO_2^-,eq,T} p_{O_2,eq}^{0.5}} = \frac{n_{NO_3^-,eq,T}}{n_{NO_2^-,eq,T}} p_{O_2,eq}^{-0.5} = x_{(1),T,p_{O_2}} p_{O_2,eq}^{-0.5} \quad (5)$$

$$\mathrm{K}_T = exp\left(-\frac{\Delta H - T \cdot \Delta S}{RT}\right) \quad (6)$$

Table 1. Thermodynamics of reaction (1). The chemical equilibrium was investigated by the authors listed in column 1. Column 2 shows the composition of the cations. Column 3 and 4 give the enthalpy ΔH and the entropy ΔS of reaction (1). The equilibrium constants at 500 °C $K_{(1),500}$ are calculated according to equation (6). The molar ratios nitrate-to-nitrite at a temperature of 500 °C and an oxygen partial pressure of 0.2 atm $x_{(1),500,0.2}$ are given in column 6.

Reference	Cation composition	Enthalpy ΔH /kJ·mol^{-1}	Entropy ΔS /J·mol^{-1}·K^{-1}	$K_{(1),500}$ /atm$^{-0.5}$	$x_{(1),500,0.2}$ /mol·mol^{-1}
[17]	Na	-101.0	-101.1	35	16
[18]	K	-115 +/- 5	-102 +/- 5	276	124
[19]	$Na_{0.64}K_{0.36}$	-115.2	-105.9	178	80
[20]	$Na_{0.5}K_{0.5}$	-94.9	-84.4	101	45

For thermal decomposition processes it is not only important to understand the equilibrium constant of equation (1) but also the reaction kinetics, if the temperature is increased or decreased. The reaction kinetics of reaction (1) with sodium and potassium cations were investigated by Freeman [7,17], Bond and Jacobs [11], Paniccia and Zambonin [12], and Nissen and Meeker [20]. These publications are compared in a condensed form in Table 2. Freeman [7,17] executed 100 mg-scale thermobalance experiments to measure the kinetics of the nitrite oxidation reaction (reverse reaction (1)). He observed the oxygen gas volume consumed by a nitrite melt (cations: sodium and potassium) in an atmosphere of oxygen (1 atm). He assumed that two nitrite ions are transformed into two nitrate ions per consumed oxygen molecule according to the reverse reaction (1). Bond and Jacobs [11] made use of the measured weight loss from an automatically recording thermobalance for kinetic calculations. They investigated the reduction of sodium nitrate to sodium nitrite (see reaction (1)) in air and in argon at 100 mg-scale. The weight loss is ascribed to the release of oxygen into the gas phase and represents the progress of the reduction reaction. Paniccia and Zambonin [12] investigated the oxidation of nitrite in about 200 g of an equimolar mixture of $NaNO_3$ and KNO_3 with 0.2 to 0.5 molar $NaNO_2$. Nitrite is produced in the nitrate melt during vacuum degassing because the steady removal of oxygen favors reaction (1). Following this, oxygen is introduced, and the apparatus is immediately flame-sealed. The measured pressure drop over time can be related to the amount of oxidized nitrite over time, assuming that all oxygen that dissolves in the melt oxidizes nitrite to nitrate. Nissen and Meeker [20] investigated the oxidation reaction kinetics in a 700 g-scale equimolar mixture of $NaNO_3$ and KNO_3 in an atmosphere with varying oxygen partial pressure from 0.33 to 1.0 atm. A certain initial nitrite concentration that is higher than its equilibrium concentration was generated by argon bubbling through the melt before starting the kinetic measurements. Measurement data was recorded in the form of nitrite concentration versus time. The nitrite concentration was measured via a titrimetric method. The five mentioned publications are compared in a condensed form in table 1. With regard to the investigated temperature range (Table 2, column 2), only the experiments Nissen and Meeker [20] meet the current operating conditions of sensible heat storage in Solar Salt. The experiments of Freeman [7] and Paniccia and Zambonin [12] touch the upper temperature limit of around 560 °C. The emphasis of Table 2 is also on the chosen experimental scales (Table 2, column 2), which vary from 100 mg to 700 g-scale, and on the investigated reaction direction (Table 2, column 3). Amongst all authors, only Bond and Jacobs followed the reduction reaction.

Table 2. Literature in the field of reaction kinetics of the nitrate/nitrite-reaction. The experimental conditions (scale, cationic species (sodium and/or potassium), initial ratio nitrite-to-nitrate, measured variable) are defined in column 2. Column 3 differentiates between experimental setups that measure the oxidation reaction (ox.), and thoses measuring the reduction reaction (red.). The activation energies are listed in column 4.

Author(s) and year	Experiment, measurement data	Oxidation or reduction	Activation Energy E_a /kcal·mol^{-1}
Freeman 1956 [17]	thermobalance, 100 mg-scale, $NaNO_2$, 1 atm O_2, 600, 650 and 700 °C, consumed O_2-volume	ox.	20.7
Freeman 1957 [7]	thermobalance, 100 mg-scale, KNO_2, 1 atm O_2, 550 to 750 °C consumed O_2-volume	ox.	34.3
Bond and Jacobs 1966 [11]	thermobalance, 100 mg-scale $NaNO_3$, air or argon, 628 to around 730°C weight loss	red.	40.3
Paniccia and Zambonin 1973 [12]	~200 g, (Na,K)NO_2 in equimolar (Na,K)NO_3, 0.1 to 1.2 atm O_2, 545 to 690 K, pressure drop	ox.	23.2 ±0.5
Nissen and Meeker 1983 [20]	~700 g, (Na,K)NO_2 in equimolar (Na,K)NO_3, 0.33 to 1.0 atm O_2, 404 and 502 °C, nitrite concentration	ox.	26.4

Freeman [7,17], Bond and Jacobs [11], and Paniccia and Zambonin [12] did not mention the possible impact of mass transport on the reaction velocity. Nissen and Meeker [20] discussed the role of oxygen mass transport as a limiting factor for the oxidation reaction. They stated that its influence was eliminated by the use of a high-speed agitator (2500 rpm) in combination with high gas flow rates (600-800 mL·min^{-1}) without bubbling of gas through the melt. Furthermore, they noted that they reproduced the oxidation rate constants of Paniccia and Zambonin, which are smaller than their own results, by deactivating the agitator and reducing the gas flow rate to 400 mL·min^{-1}.

Carling et al. [8] studied $NaNO_3$, KNO_3, and $NaNO_2$ in the 10 mg-scale with a combined TG/MS apparatus in vacuum at temperatures between 347 and 507 °C. The authors found out that a part of the salt vaporized and condensed in cooler areas. They stated that decomposition and vaporization occurred simultaneously in their experiments. Glazov and colleagues published several studies on the vapor pressures of sodium and potassium nitrate and nitrite systems. For example, Glazov et al. [9] reported vapor pressures of the system $NaNO_3$- $NaNO_2$ at 525, 550 and 575 °C. The vapor pressures for pure $NaNO_3$ are 10.01, 20.84 and 43.05 Pa, respectively. They revealed validity of Raoult's law if the concentration of one of the components is below 5 mol%.

The presented study in this paper intends to prove the applicability of thermogravimetric analysis (TG) for investigation of the nitrate/nitrite-reaction velocity. We will demonstrate a data treatment that considers mass changes due to chemical reactions and gas release, and also due to salt evaporation. TG was used in the literature to study reaction kinetics, but salt evaporation was not taken into account for data analysis so far. The investigated reaction direction is the reduction reaction, meaning the formation of nitrite and oxygen from nitrate ions. This reaction direction is considered to be the crucial one for salt stability. The reason is, that a higher temperature, e.g. in the solar receiver unit in a CSP system, shifts the chemical equilibrium towards the nitrite side (right side in equation (1)), and in that way favors the reduction reaction. Subsequently, the impact of reaction kinetics, and also of mass transport via diffusion on the velocity of the nitrite formation will be illustrated. The objective is to identify experimental sizes with mass transport limitations. Finally, the experimentally obtained velocity of the nitrite formation will be compared with simulation curves that arise from literature rate laws and kinetic parameters.

2. Experimental

The TG experiments were executed in a Netzsch STA 449 apparatus. The TG sample holder was equipped with a thermocouple type S Pt10Rh-Pt. For the 50 and 100 mg-scale experiments, the sample quantity (60 wt.% NaNO3, 40 wt.% KNO3, both >99%, Merck) was filled in a small platinum crucible, which itself was put in a larger aluminum oxide crucible to avoid spreading of the molten salt over the sample holder and other areas of the thermogravimetric system. The 700 mg sample was directly filled into the aluminum oxide crucible. Table 3 lists the labelling, masses and surface-to-volume ratios of the experiments. The apparatus was purged with synthetic air at 100 mL·min^{-1} (80 mL·min^{-1} nitrogen and 20 mL·min^{-1} oxygen, both Linde 5.0 grade) to ensure a constant oxygen partial pressure in the gas phase. The following temperature program was applied for all experiments: 1 h at 500 °C – 12 h at 450 °C – 12 h at 500 °C. A buoyancy correction curve was measured and subtracted from all measurement curves. The salt samples were subsequently analyzed via ion chromatography with regard to the nitrate and nitrite content. The analytical procedure and the Metrohm apparatus are described elsewhere [10].

Table 3. Details on the four experiment I, II, D and L. The first column gives the labels of the experiments, which are explained in column 2. Column 3 and 4 give the mass of the sample that was investigated in the TG apparatus, and the diameter of the crucible opening. The surface-to-volume ratio is calculated from the sample mass, the salt density at 500 °C ($\rho_{Na_{0.6}K_{0.4}NO_3}(500\,°C) = 1736.2\ kg \cdot m^{-3}$, [13,14]), and the crucible diameter.

Experiment label	Label meaning	Sample mass /mg	Crucible diameter /mm	Ratio $\frac{surface}{volume}$ /mm^{-1}
I	Basic scale	51.716	6.8	1.22
II	Basic scale	53.492	6.8	1.18
D	**D**ouble scale	99.417	6.8	0.63
L	**L**arger scale	697.978	15.8	0.49

The 100 g-scale experiment was executed in an autoclave test rig. For a detailed description of the test rig, see reference [10]. The gas space was purged at a gas flow rate of 200 mL·min^{-1} with synthetic air above the melt (80 vol.% nitrogen, 20 vol.% oxygen) in order to ensure a constant oxygen partial pressure in the gas phase. When the melt reached a temperature of 300 °C that is well above the melting temperature, a stirrer was switched on. Once, the experiments reached 500 °C the experiment started (time zero) and a first salt sample was taken. Further samples were taken regularly. The total timeframe of the experiment was 6 days.

3. Modeling

The simulation curves were calculated using the COMSOL software package (version 5.2a). The implemented differential equation was derived from the literature [20]. The simulation is based on the published equation (7) with the oxidation rate constant (k_1) and reduction rate constant (k_{-1}), as well as the nitrite and nitrate concentrations $[NO_2^-]$ and $[NO_3^-]$ (unit: mol·kg^{-1}) and the oxygen partial pressure $[O_2]$ (unit: atm). It is not possible to derive a model equation for the reduction reaction from the Freeman publication[17], because the proposed rate law is only valid at 1 atm oxygen partial pressure. The rate law of Bond and Jacobs [11] is not valid in the range of mass change that is investigated in this study. Also, the Paniccia and Zambonin [12] publication cannot be used for modelling, because the proposed rate law only describes the oxidation reaction.

$$-\frac{d[NO_2^-]}{dt} = k_1[NO_2^-][O_2] - k_{-1}[NO_3^-] \tag{7}$$

A 0D-model is chosen for the simulations meaning that concentrations are supposed to be constant in all directions of space. It is assumed that the melt volume V is not affected by the nitrate/nitrite-reaction, which is justified because of the high equilibrium molar ratio nitrate-to-nitrite. This assumption is implemented in the model by equal molar volumes ($v_i = V_i/n_i = M_i/\rho_i$, $M_{Na_{0.6}K_{0.4}NO_3} = 91.4\ g \cdot mol^{-1}$, $M_{Na_{0.6}K_{0.4}NO_2} = 75.4\ g \cdot mol^{-1}$, $\rho_{Na_{0.6}K_{0.4}NO_3}(500\ °C) = 1736.2\ kg \cdot m^{-3}$ [13,14]) of nitrate and nitrite. The model assumes constant oxygen concentration over time. The rate law of Nissen [20] includes the oxygen partial pressure (instead of e.g. the oxygen concentration in the melt; both are linked via Henrys law). Calculations are made with an oxygen partial pressure p_{O_2} of 0.2 atm. The model equations are noted in equation (8) and (9). The concentration change over time is expressed in equation (8) in terms of the reaction rate R_i of the regarded species i. The reaction rates are specified further in equation (9) in terms of the actual concentrations c_i of the reacting species, and in terms of the rate constants k. The rate constants at 500 °C were calculated from Arrhenius fits of the published rate constants [20], according to $k_{ox} = 6375\ s^{-1} \cdot \exp(-\frac{114.8\ \frac{kJ}{mol}}{RT})$, $k_{red} = k_{ox}/K$, $K = exp(-\frac{-94.9\ \frac{kJ}{mol} - T \cdot -84.4\ \frac{J}{mol \cdot K}}{RT})$. The temperature was hold at 450 °C for 550 h to allow chemical equilibrium at this temperature, and at 500 °C for 140 h.

$$\frac{dc_i}{dt} = R_i \tag{8}$$

$$R_{NO_3^-} = -(c_{NO_3^-}k_{red} - c_{NO_2^-}p_{O_2}k_{ox}) \qquad R_{NO_2^-} = +(c_{NO_3^-}k_{red} - c_{NO_2^-}p_{O_2}k_{ox}) \tag{9}$$

The simulation results, given as concentration of nitrite $c_{Na_{0.6}K_{0.4}NO_2}$ (unit: mol·m^{-3}) are transformed into a mass loss Δm (unit: wt.%) via equation (10). The calculation refers to the stoichiometry of reaction equation (1). 0.5 oxygen molecules O_2 ($M_O = 16.0\ g \cdot mol^{-1}$) are released from the melt per formed nitrite ion and in that way reduces that sample mass over time.

$$\Delta m(t) = \frac{c_{Na_{0.6}K_{0.4}NO_2}(t) \cdot M_O}{\rho_{Na_{0.6}K_{0.4}NO_3}} \cdot 100\% \tag{10}$$

4. Results and Discussion

Figure 1a shows the mass change curves of the 50, 100, and 700 mg experiments. A buoyancy correction curve was subtracted from all curves. The shape of the 500 °C-12 h segment is similar in all measurements. The mass change rate is fast in the beginning of this segment (Figure 1a, 500-12-I), and slows down over time. Eventually, it reaches a steady value meaning that the curve is of linear shape (Figure 1a, 500-12-II). The linear regime is reached after a notably shorter time period in the 50 mg experiments (green and blue curve, I and II) than in the larger scale experiments (orange curve, L). Typically, the kinetics of a reversible chemical reaction with gas consumption or release leads to an exponentially shaped mass change curve [15,16], which conforms the observation in 500-12-I. However, a mass change rate of zero is expected to establish after some time, when the chemical equilibrium of the reaction is reached. Instead, we observe a constant mass change rate in the 500-12-II regime for the experiments.

Two physico-chemical phenomena are the most probable explanations for this observation: Additional chemical reactions and salt evaporation. First, a second chemical reaction could occur in the melt, e.g. the formation of nitrous gases from nitrite ions (see equation (2), (3) or (4)). Due to steady removal of the formed gases by the purge flow, such a reaction cannot achieve chemical equilibrium and causes a steady mass loss. However, all reactions that produce nitrous gases simultaneously form oxide ions in the melt. The 700 mg sample (L) was analyzed by a titrimetric method with regard to oxide ions after the TG experiment, and no oxide ions were found. A second

chemical reaction was therefore considered as irrelevant. Second, the steady mass loss could arise from salt evaporation. As mentioned in the literature section of this paper, salt evaporation was observed and investigated in the past. Since the phenomenon depends on the surface-to-volume ratio it may well explain the different slopes in the 500-12-II regime. The 50 mg-experiments have relatively high surface-to-volume ratios, and the mass change rate is high compared to the larger scale experiments. Hence, salt evaporation is regarded as the most probable explanation for the 500-12-II regime.

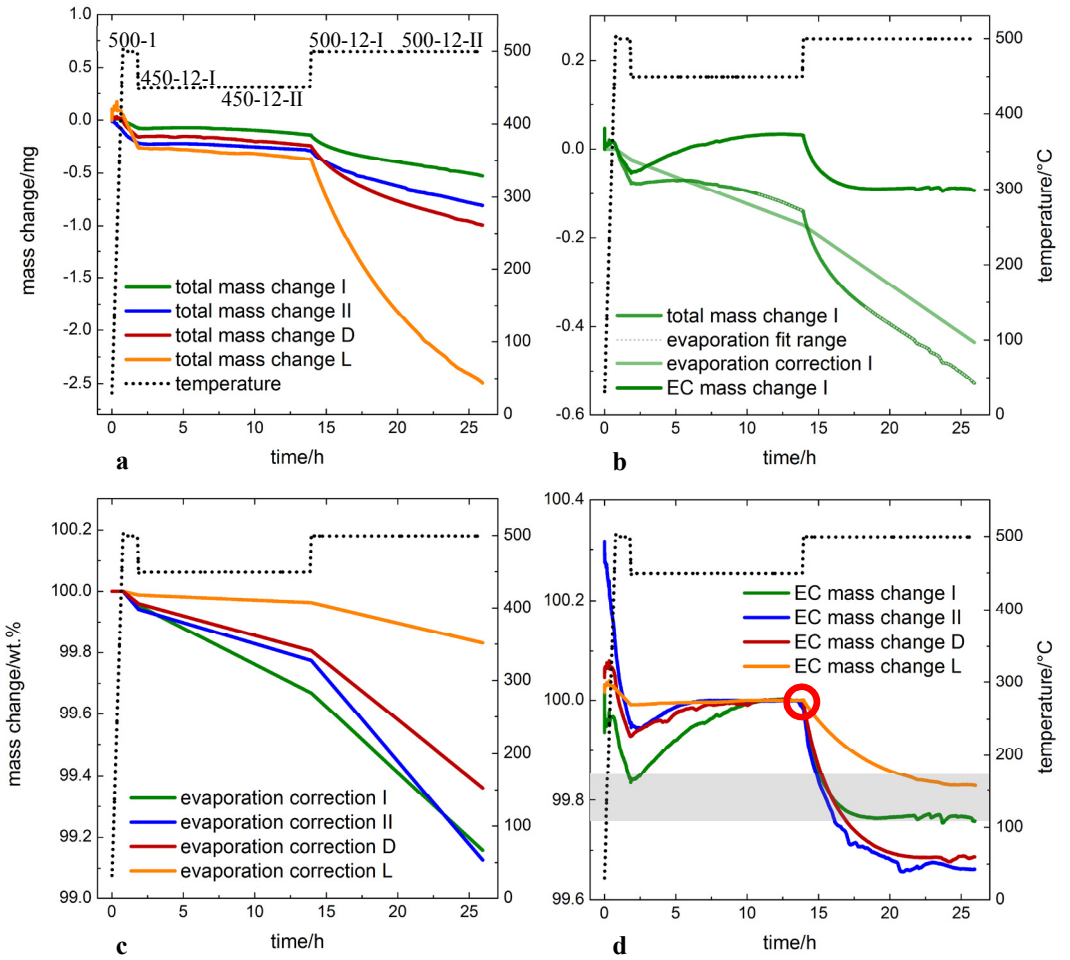

Figure 1. Data and data treatment of the TG experiments. The black dotted curves always show the temperature profile. The abbreviations I, II, D and L refer to the 50 (I and II), 100 (D means double sample mass), and 700 mg-scale (L means larger scale) experiments. Note that the mass change is given in mg in the upper two diagrams, whereas the unit changes to wt.% in the lower diagrams. a: Experimentally measured mass change curves. A buoyancy correction curve was subtracted from all curves. The term 'total mass change' refers to the assumption, that the measured mass change can be divided into a part that is based on a chemical reaction, and a part that is caused by salt evaporation. The labels on the temperature curves denote the sequences of the temperature program. For example, 500-12-I denotes the first part of the sequence where temperature is kept at 500 °C for 12 h. b: Exemplary illustration of the evaporation correction procedure. The EC mass change (means evaporation corrected mass change) curve is the result of subtracting the evaporation correction from the total mass change. The evaporation correction curve images the mass change that is caused by salt evaporation. c: Diagram of the evaporation correction curves. d: Diagram of the EC mass change curves. Note that zero point on the y-axis (mass change-axis) is chosen arbitrarily in order to achieve good comparability. The curves were shifted along the y-axis until they coincided at the very end of the 450-12 segment (see red circle), and this point was declared to be 0 wt.% mass change. The grey area is restricted by mass changes that are calculated from the literature data (Tracey 1978, Nissen 1983] in Table 2.

The following procedure aims for transforming the experimentally measured mass change curves (Figure 1a) into corrected mass change curves that only depict the mass change that is based on the nitrate/nitrite-reaction, but no longer the mass change caused by salt evaporation. The procedure is reasonable under the assumption that the nitrate/nitrite-reaction (1) proceeds over a certain limited time period and reaches equilibrium at some point, whereas salt evaporation is constant during isotherms. The procedure is illustrated exemplarily for experiment I in Figure 1b. Salt evaporation rates are calculated from the linear 500-12-II regimes, and also from the linear part of the 450-12-II segment (see dotted part of the total mass change curve in Figure 1b), where mass loss is solely based on salt evaporation. The rates are listed in Table 4 for all four experiments. Evaporation correction curves are calculated from these values. The total mass was set to zero when the 500 °C-1 h segment (500-1) begins. Figure 1c shows the evaporation correction curves. Each curve is steeper in the 500-1 and 500-12 segment than in the 450-12 segment because a higher temperature accelerates salt evaporation. Comparison of the evaporation correction I and II reveals that the evaporation rate of experiment II is 41% smaller and 27% higher than in experiment I at 450 and 500 °C, respectively, even though the sample mass and consequently the ratio surface-to-volume are similar. We consider this difference to be within the accuracy of the balance in the TG apparatus, which has to resolve mass changes that are in the range of a few µg (or a few hundredth wt.%). The evaporation rates of experiment D are 32% (450 °C) and 23% (500 °C) smaller than the corresponding average of experiment I and II. Also, the evaporation rates of experiment D are smaller than the individual evaporation rates of experiment I and II at the same temperature. This result can be judged as a slight tendency towards a dependency of evaporation rate and surface-to-volume ratio (which is approximately twice as high for experiments I and II, compared to experiment D). Despite, results have to be taken with care, since deviation of the results of experiment I and II (-41% and +27%) are higher than the difference to experiment D (-32% and -23%). The evaporation rates of experiment L are 89% (450 °C) and 77% (500 °C) smaller than the corresponding average of experiment I and II. These percentages are significantly higher than the deviation of the experiment I and II results. Apparently, the influence of the smaller surface-to-volume ratio on the evaporation rate is qualitatively observable in experiment L, compared to the smaller scale experiments.

Table 4. Evaporation rates at 450 and 500 °C determined by TG analysis. The linear parts of experimentally measured mass change curves are fitted according to the equation $y = i + s \cdot x$, where the slope s corresponds to the evaporation rate. R^2 (column 4 and 6) is the coefficient of determination of each fit.

		450 °C		500 °C	
Experiment	**Ratio $\frac{surface}{volume}$ /mm^{-1}**	**Evaporation rate /wt.%·min^{-1}**	**R^2**	**Evaporation rate /wt.%·min^{-1}**	**R^2**
I	1.22	$3.9 \cdot 10^{-4}$	0.9966	$7.1 \cdot 10^{-4}$	0.9990
II	1.18	$2.3 \cdot 10^{-4}$	0.9998	$9.0 \cdot 10^{-4}$	0.9958
D	0.63	$2.1 \cdot 10^{-4}$	0.9983	$6.2 \cdot 10^{-4}$	0.9947
L	0.49	$3.4 \cdot 10^{-5}$	0.9988	$1.8 \cdot 10^{-4}$	0.9973

The evaporation correction curves were subtracted from the total mass change curves, see e.g. Figure 1b, where the evaporation correction curve of experiment I is subtracted from the total mass change curve resulting in the EC mass change curve (EC signifies **e**vaporation **c**orrected mass change). All EC curves are shown in Figure 1d.

The mass change in the 500-12 segment varies by 0.2 wt.%, when all four experiments are compared. At the same time, ion chromatography analysis of the salt samples (each after the TG experiment) reveals that the mass change due to oxygen release at 500 °C is between 0.36 wt.% (experiment L) and 0.41 wt.% (experiment D), that is a variation by only 0.05 wt.% (calculation based on the values of Table 5, column 4). Apparently, the deviation along the mass change-axis (y-axis) is relatively large when the experiments are compared amongst each other, which was already mentioned in the context of evaporation rates. In contrast, the fluctuations in the individual curves are relatively small. Evidence for the large deviation amongst the experiments and the small fluctuations in each curve becomes obvious, when the total mass change I and II in Figure 1a are regarded. The two curves are

significantly shifted relative to each other along the y-axis, whereas fluctuations in each curve are comparably small.

Table 5. Ion chromatography post analysis results of the TG samples. Column 3 and 4 gives the ion concentrations as amount of substance nitrate or nitrite relative to the total salt mass. The molar ratio in column 6 is calculated by dividing the molar concentrations. The molar ratios $x_{(1),500,0.2}$ can be compared to literature, where values of 80 mol·mol^{-1} [19] and 45 mol·mol^{-1} [20] are found.

Experiment	Ratio $\frac{surface}{volume}$ /mm^{-1}	Nitrate concentration /mol·kg^{-1}	Nitrite concentration /mol·kg^{-1}	K	$x_{(1),500,0.2}$ /mol·mol^{-1}
I	1.22	11.1	0.234	106	47
II	1.18	11.0	0.231	106	48
D	0.63	11.0	0.256	96	43
L	0.49	11.0	0.225	109	49

The mass change that occurs when temperature changes from 450 to 500 °C can also be calculated from the thermodynamic parameters listed in Table 1. It amounts to 0.73, 0.09, 0.15, and 0.24 wt.% according to the data of Freeman [17], Bartolomew [18], Tracey et al. [19], and Nissen and Meeker [20]. The latter two are considered as appropriate for comparisons because their cation compositions are similar or equal to the one in Solar Salt. The two values are illustrated in Figure 1d as upper and lower border of the grey area. The mass change of the experiments I and L meet the mass change predicted from literature, whereas experiment II and D show higher mass changes that predicted. However, the orders of magnitude of the mass changes of all curves are consistent with the predicted values. Furthermore, the deviations of the measured mass changes in this study from the closest literature value are as small as the difference of the two literature values, both being around 0.1 wt.%. Overall, plausibility of the total mass changes of all TG-experiments is given, and the curves can be used further for discussion of the reaction velocity.

The following discussion focuses on the velocity of the nitrate/nitrite-reaction when the melt is heated from 450 to 500 °C using Figure 1d. The Segments 500-1 and 450-12 are applied to achieve chemical equilibrium at 450 °C. It is assumed that all samples have the same composition, including concentrations of nitrate and nitrite ions, at the end of the 450-12 segment. When temperature is increased to 500 °C, the chemical equilibrium is shifted towards a higher nitrite concentration, and the reduction reaction (1) proceeds. The thereby formed oxygen is released from the melt, and the sample mass decreases. Chemical equilibrium at 500 °C is reached, when the mass is constant again. A certain period of time $\Delta t_{450/500}$ is required until the system reaches chemical equilibrium again, when temperature is increased by 50 °C. These periods of time can be compared qualitatively in this study. $\Delta t_{450/500}$ of the experiments I and II are expected to be equal, because the surface-to-volume ratios are similar (1.22 and 1.18 in experiment I and II, respectively). In Figure 1d it seems that experiment I (green curve) reaches equilibrium slightly faster than experiment II (blue curve). This deviation may be due to small inhomogeneities in the melt, or due to inhomogeneous heating. $\Delta t_{450/500}$ of experiment D is equal to $\Delta t_{450/500}$ of the experiments I and II, when the deviation of experiment I and II is taken into account. Obviously, the smaller surface-to-volume ratio in experiment D, compared to experiment I and II, does not influence the reaction velocity. Consequently, mass transport of oxygen through the melt is still fast enough in the 100 mg-scale experiment (D) and is not the limiting factor for reaction velocity. We conclude that experiment I, II and D all show pure reaction kinetics without mass transport limitations. In contrast, $\Delta t_{450/500}$ of experiment L is significantly longer. Apparently, the reaction velocity is not only determined by reaction kinetics, but also by mass transport. Due to the relatively small surface-to-volume ratio, the formed oxygen has to diffuse for a longer distance through the melt before it is released to the gas phase. In this work, the melt can be viewed as a 'sponge' that stores the oxygen for a certain time. As a consequence, the chemical equilibrium is temporarily and locally shifted to a lower nitrite concentration, and slows down the reduction reaction.

Finally, experiments I, II, D and L are compared to a larger scale experiment (100 g) and the simulation curve, see Figure 2. The 50 and 100 mg-scale experiments (I, II and D) require between around 2 to 7 hours (see Figure 1d or Figure 2 lower part) until chemical equilibrium is reached at 500 °C. The 700 mg-scale experiment (L) needs

about 10 hours, and the 100 g-scale experiment needs around 100 hours (see dotted curve in the upper part of Figure 2). The simulation curve, which is based on the kinetic model of Nissen and Meeker [20] lies in between the 700 mg and the 100 g-scale experiments. Probably, Nissen and Meeker could not exclude mass transport effects in their 700 g-scale experiments, even though the stirring rate was high. Another point is that they investigated the oxidation reaction, whereas the simulation in this study describes the reduction reaction. In principle, the published rate law is valid for both directions of the nitrate/nitrite-reaction, but yet this difference can be considered as a source of errors. For future simulations, we propose to take into account both reaction kinetics and mass transport phenomena, especially when simulation of larger scale facilities is intended.

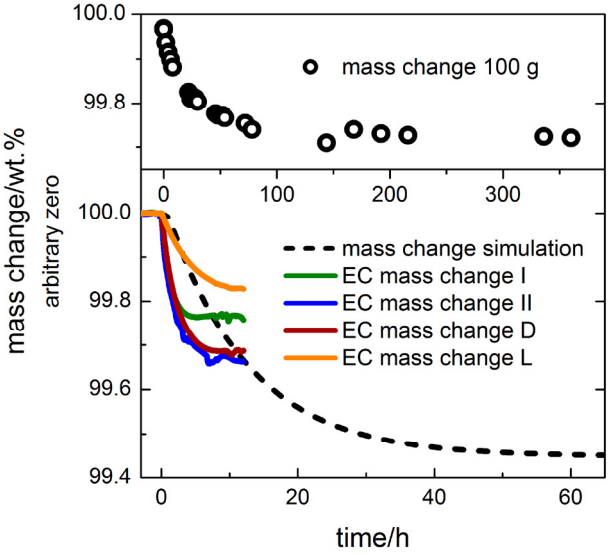

Figure 2. Comparison of mass changes in numerical simulation, mg-scale experiments (TG), and 100 g-scale experiment. The lower x-axis (time-axis) is valid for the EC mass change curves (TG), and for the simulation curve. The upper x-axis (time-axis) is valid for the 100 g curve. For better comparability, time was set to zero at the beginning of the 500 °C period for all curves.

5. Summary and Conclusion

The present study demonstrates that thermogravimetric analysis is an appropriate method for the investigation of reaction kinetics of the nitrate/nitrite-reaction at 500 °C in Solar Salt. The data treatment is based on the assumption that the considered nitrate/nitrite-reaction proceeds for a certain limited time frame and reaches equilibrium at some point, whereas salt evaporation is constant at a given temperature. In the linear regimes of the curves, the measured mass loss is found to be solely based on salt evaporation. The influence of the surface-to-volume ratio on the evaporation rate was qualitatively observable in the presented experiments. Curve correction by subtracting the evaporation mass loss successfully separates the salt evaporation mass loss, and gives the pure reaction mass loss curve. The total mass change that occurs when the melt temperature is changed from 450 to 500 °C and nitrate decomposes to nitrite is reasonable and comparable to equilibrium data calculated from literature. It could be shown, that the surface-to-volume ratio clearly affects the velocity of the nitrite formation. The time that is needed until chemical equilibrium is reached decreases with increasing surface-to-volume ratio up to a certain critical ratio that will be determined with future experiments. It can be concluded, that the existing literature of larger scale experiments may not describe solely kinetics but rather a reaction velocity of the nitrite formation including also mass transport limitations. The conclusions about the nitrate/nitrite-reaction in Solar Salt are supported by equilibrium calculations, ion chromatography measurements, experiments at different scales (thermogravimetric analysis: 50 to 700 mg, autoclave test rig: 100 g) and kinetic modeling presented in this paper.

Acknowledgements

The authors thank the German Federal Ministry for Economic Affairs and Energy for the financial support given to this work in the MS-STORE project (Contract No. 0325497 A). Technical assistance from Markus Braun (DLR Stuttgart) is greatly appreciated.

References

[1] Tian Y, Zhao CY. "A review of solar collectors and thermal energy storage in solar thermal applications." *Applied Energy* (2013);104:538–553.
[2] Mehos M, Turchi C, Vidal J, Wagner M, Ma Z, Ho C, et al. "Concentrating solar power Gen3 demonstration roadmap." NREL (National Renewable Energy Laboratory (NREL), Golden, CO (United States)) (2017).
[3] Hoshino Y, Utsunomiya T, Abe O. "The Thermal Decomposition of Sodium Nitrate and the Effects of Several Oxides on the Decomposition." *The Chemical Society of Japan* (1981);54:1385–1391.
[4] Lee AKK, Johnson EF. "The Stoichiometry and Kinetics of the Thermal Decomposition of Molten Anhydrous Lithium Nitrite." *Inorganic Chemistry* (1972);11:782–787.
[5] Protsenko PI, Bordyushkova EA. "Kinetics and mechanism of the thermal dissociation of the nitrites of calcium, strontium, and barium." *Russian Journal of Physical Chemistry* (1965);39:1048–1051.
[6] Wei D, Wang Y, Peng Q, Yang X, Ding J. "NOx emissions and NO2- formation in thermal energy storage process of binary molten nitrate salts." *Energy* (2014);74:215–221.
[7] Freeman ES. "The Kinetics of the Thermal Decomposition of Potassium Nitrate and of the Reaction between Potassium Nitrite and Oxygen." *Journal of the American Chemical Society* (1957);79.
[8] Carling RW. "Heat capacities of NaNO3 and KNO3 from 350 to 800 K." Thermoch (1983);60:265–275.
[9] Glazov VI, Dukhanin GP, Dkhaibe MK. "Saturated Vapor Pressure over the Melts of the NaNO2NaNO3 System." *Russian Journal of Applied Chemistry* (2003);76:1405–1407.
[10] Bonk A, Martin C, Braun M, Bauer T. "Material Investigations on the Thermal Stability of Solar Salt and Potential Filler Materials for Molten Salt Storage." *Solar Paces* (2016).
[11] Bond BD, Jacobs PWM. "The Thermal Decomposition of Sodium Nitrate." *Journal of the Chemical Society* (1966);A:1265–1268.
[12] Paniccia F, Zambonin PG. "Redox Mechanisms in an Ionic Matrix. III. Kinetics of the Reaction N02- + 1/2 O2 = NO3- in Molten Alkali Nitrates." *The Journal of Physical Chemistry* (1973);77:1810–1813.
[13] Janz GJ, Allen CB, Bansal N, Murphy R, Tomkins R. "Physical properties data compilations relevant to energy storage. II. Molten salts: data on single and multi-component salt systems." National Standard Reference Data System (1979).
[14] Pacheco JE, Ralph ME, Chavez JM, Dunkin SR, Rush EE, Ghanbari CM, et al. "Results of molten salt panel and component experiments for solar central receivers: cold fill, freeze/thaw, thermal cycling and shock, and instrumentation tests." Sandia National Labs., Albuquerque, NM (United States) (1995).
[15] Connors KA. Chemical kinetics: The study of reaction rates in solution. John Wiley & Sons; 1990.
[16] Quack M, Jans-Buerli S. "Molekulare Thermodynamik und Kinetik, Teil 1: Chemische Reaktionskinetik." Verlag Der Fachvereine, Zuerich (1986).
[17] Freeman ES. "The kinetics of the thermal decomposition of sodium nitrate and of the reaction between sodium nitrite and oxygen." *The Journal of Physical Chemistry* (1956);60:1487–1493.
[18] Bartholomew RF. "A Study of the Equilibrium KNO3(l)=KNO2(l)+1/2O2(g) over the Temperature Range 550-750°." *The Journal of Physical Chemistry* (1966):3442–3446.
[19] Tracey T. "Conceptual Design of Advanced Central Receiver Power System." Martin Marietta Corporation, Final Report for Contract EG77-C-03-1724 (1978).
[20] Nissen DA, Meeker DE. "Nitrate/Nitrite Chemistry in NaN03-KN03 Melts." *Inorganic Chemistry* (1983);22:716–721.